AJNR

Theoretical Basis of Hemodynamic MR Imaging Techniques to Measure Cerebral Blood Volume, Cerebral Blood Flow, and Permeability

G. Zaharchuk

AJNR Am J Neuroradiol 2007, 28 (10) 1850-1858
doi: https://doi.org/10.3174/ajnr.A0831
http://www.ajnr.org/content/28/10/1850

PHYSICS REVIEW

Theoretical Basis of Hemodynamic MR Imaging Techniques to Measure Cerebral Blood Volume, Cerebral Blood Flow, and Permeability

G. Zaharchuk

SUMMARY: Cerebrovascular hemodynamic assessment adds new information to standard anatomic MR imaging and improves patient care. This article reviews the theoretic underpinnings of several potentially quantitative MR imaging–based methods that shed light on the hemodynamic status of the brain, including cerebral blood flow (CBF), cerebral blood volume (CBV), and contrast agent permeability. Techniques addressed include dynamic susceptibility contrast (which most simply and accurately estimates CBV), arterial spin labeling (a powerful method to measure CBF), and contrast-enhanced methods to derive permeability parameters such as the transport constant K_{trans}.

The study of cerebral hemodynamics has a long history, stretching back to the fundamental recognition by Wepfer in the 1600s that ischemic stroke was a vascular disease. The brain is an unusual organ in the hemodynamic sense, with a high metabolic rate that is sustained through high cerebral blood flow (CBF) (50 mL blood per minute per 100 g); however, unlike other high-flow organs, the limited space inside the bony cranium requires an efficient regulation system, which is accomplished with a high capillary density but remarkably low cerebral blood volume (CBV), on the order of 2–5 mL/100 g. Because of this, dysregulations of flow and volume even for short periods can have protean consequences.

Changes in hemodynamic parameters can precede abnormalities on conventional MR imaging, and knowledge of whether a lesion identified on anatomic imaging sequences is associated with increased or decreased CBF or CBV can frequently help narrow the differential diagnosis. Additionally, measurement of contrast agent permeability, such as a transport constant related to the permeability–surface area (K_{trans}) and the fractional volume of the extravascular extracellular space (v_e), may be useful to evaluate diverse brain diseases such as multiple sclerosis, ischemia, and brain neoplasms. Given their relationship with underlying biology, they have been proposed to be sensitive biomarkers to assess medical or surgical therapies.

Dynamic Susceptibility Contrast: Also Known as Bolus Perfusion-Weighted Imaging

Gadolinium chelates with high magnetic susceptibility were developed in the mid 1980s for use as MR imaging contrast agents. Given their size and low lipophilicity, they are constrained to the intravascular space by a normal blood-brain barrier (BBB). In common clinical practice, they are injected slowly through a peripheral vein; then, images are acquired after several minutes to visualize the well-recognized parenchymal enhancement that occurs in regions of BBB breakdown.

These agents can be used in a different way, as "tracers," by injecting them as tight intravenous (IV) boluses and then imaging their initial passage through the brain vasculature. This requires larger gauge IV catheters and higher injection rates ($\geq$4 mL/s), coupled with repeated rapid cine imaging of a volume of interest while the contrast passes through the capillary network. To record the tracer concentration during this passage faithfully, one must acquire images at a rate faster than the time it takes the bolus to pass through the tissue, which is usually on the order of several seconds. This acquisition requires rapid imaging sequences such as Cartesian or spiral echo-planar imaging (EPI). Images are first acquired to determine the baseline signal intensity of each voxel. When the bolus passes through the voxel, the signal intensity drops (Fig 1). This drop occurs because the contrast agent is confined to the vascular space, which creates microscopic variation in the local magnetic field, which directly leads to decreased signal intensity on gradient-echo images. The intravascular contrast also creates magnetic field gradients around the vessel, which cause signal-intensity loss when protons diffuse in these gradients.[1] One can quantify the change in transverse relaxivity (ΔR2 or ΔR2*, for spin-echo or gradient-echo, respectively) at each time point and in each voxel as

$$\Delta R2(t),\ \Delta R2^{\star}(t) = \frac{-1}{TE}\ln\left(\frac{S(t)}{S_0}\right), \quad 1)$$

where $S(t)$ is the signal intensity in the voxel at time t and S_0 is the baseline signal intensity before the bolus arrives. This relaxivity change is assumed to be linearly proportional to the tissue contrast agent concentration (though this assumption has been questioned recently[2]) and confined within the intravascular space without leakage. It has been suggested that the effects of extravasation can be minimized with the application of a preloading dose of contrast agent[3] or by using multiecho methods.[4,5] More complex modeling has been undertaken to parse out the separate effects of permeability, and some of these methods are discussed in the section on permeability imaging.

Theoretic simulations have demonstrated that R2* changes are not affected by vessel size; thus, gradient-echo perfusion-weighted imaging (PWI) includes contributions from all the vessels within the voxel.[1,6] Spin-echo PWI, though having approximately a threefold lower signal-to-noise ratio (SNR) than gradient-echo PWI, is relatively more sensitive to capillary vessels. Thus, spin-echo PWI allows insight into processes on the microvascular level while suppressing the effects of larger vessels. The behavior of spin-echo– and gradient-echo–

From the Neuroradiology Section, Stanford University Medical Center, Stanford, Calif.

Please address correspondence to Greg Zaharchuk, PhD, MD, Assistant Professor of Radiology, Neuroradiology Section, Stanford University Medical Center, 1201 Welch Rd, PS-04, Stanford, CA 94305-5487; e-mail: gregz@stanford.edu

DOI 10.3174/ajnr.A0831

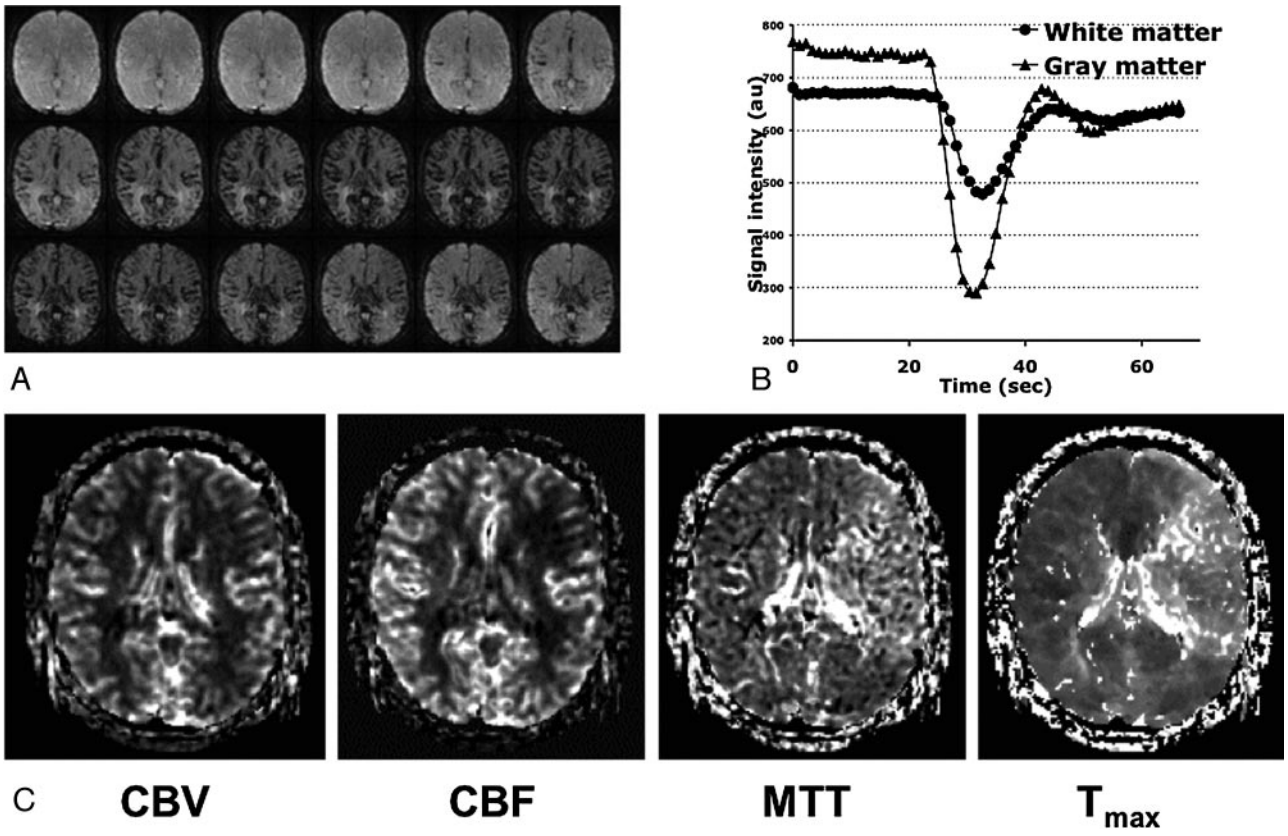

Fig 1. *A*, Time course of the signal intensity from 1 section of a multisection gradient-echo EPI dataset at 1.5T during gadopentetate dimeglumine passage, TR/TE = 1,125/49 ms. During the first pass, signal intensity decreases due to the microscopic field-strength variations and water diffusion through gradients created by the intravascular contrast agent. *B*, Signal intensity versus time for regions of interest in the gray and white matter. *C*, From these curves and an estimate of the AIF, maps of perfusion-weighted parameters such as CBV, CBF, MTT, and T_{max} can be created. Note the prolonged MTT and T_{max} in the left hemisphere, representing ischemic tissue within the left middle cerebral artery territory. Sec indicates seconds; au, arbitrary units. Image courtesy of Dr. Rexford Newbould, Stanford University.

derived measures of CBV differs in animal models of ischemia and brain neoplasms.[7-9]

Quantifying Hemodynamics with Bolus PWI

Tracer kinetic theory states that if one knows the input and the output of a tracer from a voxel, one can determine the volume of distribution (ie, CBV, or more strictly in this case, the plasma volume, because the contrast is excluded from the red blood cells) and the clearance rate (CBF) by using conservation of mass mathematics.[10] Such methods were applied by using inert tracer dyes to calculate global flow rates to organs in the 1940s.[11] However, in imaging, there are 2 crucial differences: We are interested in focal rather than global measurements[1] and we do not strictly know either the input or output from any voxel, that would be needed to apply off-the-shelf tracer kinetic equations.[2] The 1 piece of information that we do have is the signal-intensity changes in all the voxels, from which we can estimate the plasma and tissue tracer concentration.

Ignoring recirculation, one can measure plasma volume (v_p = CBV · [1 − hematocrit (Hct)]) as the integral of the tissue concentration time curve:

$$2) \qquad \nu_p \propto \int_0^\infty C_{tissue}(t)dt$$

This can theoretically be made quantitative by dividing by the value of this integral in a voxel that is known to contain 100% blood:

$$3) \qquad \nu_p = \frac{\int_0^\infty C_{tissue}(t)dt}{\int_0^\infty C_{blood}(t)dt}$$

with the assumption that the large and small vessel Hcts are equal.[12]

Strictly, recirculation effects should be recognized and removed from the curves. In reality, unless there is significant BBB permeability or areas of very low flow, recirculation effects may be ignored and actually lead to improved estimates of plasma volume that are less sensitive to contrast agent delivery rates (ie, CBF). In low-flow regions, if the tracer does not complete its first passage within the time given for the measurement (usually about 25–30 seconds), it will be undercounted and v_p will be underestimated. Because of this result, some authors writing about ischemia have used the term "perfused CBV".[13] This may account for the discrepancies seen in between PWI and $C^{15}O$ PET estimates of CBV in ischemia.[14] In fact, in the extreme, one would prefer to image as late after injection as possible; when the contrast agent concentration is

changing slowly, it more closely approximates a steady-state or "blood pool" measurement, which is independent of flow.[15] However, this results in unacceptably low SNR at 1.5T. Such an approach may be feasible by using triple-dose contrast at higher field strengths.

To measure CBF, one requires knowledge about the temporal shape of the input concentration into the voxel and the tissue concentration curve.[16,17] The input concentration time curve is different for every voxel and cannot be directly measured. Because of this difference, it must be estimated. The most traditional approach is to measure the contrast agent concentration curve in a large feeding artery at the base of the brain, such as the middle cerebral artery or anterior cerebral artery, and then to apply this arterial input function (AIF) to all of the voxels in the brain. More recently, attempts to define more local AIFs have been suggested.[18,19] Difficulties associated with inflow effects, partial volume averaging, vessel-orientation-dependent relaxivity, and possible differences in relaxivity between tissue and bulk blood also make it challenging to determine the true AIF concentration, which is critical for quantitative CBF measurements.[20]

The tissue concentration curve is a combination of the effects of the AIF and the inherent tissue properties. Because of this, the effects of the AIF on the tissue concentration curve must be removed, a process known mathematically as deconvolution. The most commonly used deconvolution methods are "nonparametric," which means they do not assume a shape for the tissue response curve. The basic concept is to figure out what the tissue concentration curve would be for an idealized AIF of infinite sharpness and unit area. This is modeled as a "residue function," R(t), which plots the fraction of this infinitely sharp bolus that remains in the voxel at time t after injection (Fig 2). As such, it has a maximal value of 1 at t = 0 and monotonically decreases to zero. Given this construct, the relationship between the tissue concentration and AIF is the following:

$$4)\quad C_{tissue}(t) = CBF \cdot AIF(t) \otimes R(t) = CBF \int_0^t AIF(\tau)\, R(t-\tau)\, d\tau,$$

where $\otimes$ is the convolution operator. Because we presumably know C_{tissue} and AIF at every time *t*, the goal is to solve for *CBF* and *R(t)*. A simple and intuitive approach to solve this equation is to use the properties of the Fourier transform, where complicated convolutions become simpler multiplications:

$$5)\qquad CBF \cdot R(t) = FT^{-1}\left(\frac{FT(C_{tissue}(t))}{FT(AIF(t))}\right),$$

where *FT* and FT^{-1} represent the one-dimensional forward and inverse Fourier transforms, respectively. Because the residue function by definition is equal to 1 at $t = 0$, the magnitude of the first time point of the solution is *CBF*. This was the initial approach to solving equation (Eq) 4[21]; however, in current practice, this is not the usual approach because of the ill-posed nature of Eq 4, which frequently yields nonphysiologic oscillations in the solution for the residue function. Also, the division of 2 Fourier transformed concentration curves in Eq 5 can be quite noisy under physiologic SNR levels.

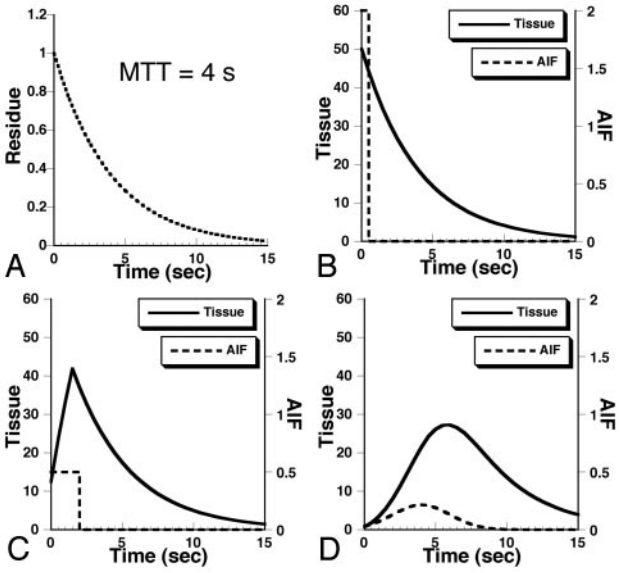

Fig 2. Effects of bolus widening ("dispersion") in the AIF on the tissue-concentration-versus-time curve. *A*, Residue function, which represents the probability of the tracer remaining in the voxel at time *t*. Note that this is a monotonically decreasing function, with a value of 1 at time $t = 0$. The residue function shown here represents a well-mixed single compartment with an MTT of 4 seconds, similar to that seen in brain. For the remainder of the examples, CBF is taken to be 50 mL/100 mL of brain per minute, again typical for brain. The area under the AIF is normalized to 1 arbitrary unit. *B*, Tissue concentration curve (solid line) for a "perfect bolus" AIF (dotted line), which arrives at $t = 0$. The tissue concentration curve is just the residue function multiplied by CBF. Note that CBF is equal to the first point of the tissue concentration curve, which is also the peak concentration. *C*, AIF is a 2-second bolus top hat function corresponding to "plug flow": note the increase in the arrival time of peak contrast and the decrease in peak concentration, a consequence of the convolution of the AIF and the residue function. No longer is CBF equal to the first time point of the tissue curve or the peak concentration. *D*, AIF is a gaussian curve with full width at half maximum of 2 seconds, a more realistic model of a bolus that has widened before reaching the tissue. Note that for both *C* and *D*, deconvolution techniques are necessary to determine CBF and that the first moment of the tissue concentration curve is not equal to the MTT. Sec indicates seconds.

A more robust method that has gained widespread acceptance is known as singular value decomposition (SVD), which requires that the previous equations be recast in terms of matrices.[17] The mathematics behind SVD deconvolution is beyond the scope of this basic review.[22]

Other methods to estimate CBF from the tissue concentration versus time curves include parametric deconvolution methods as well as nondeconvolution methods. Parametric deconvolution techniques assume a shape for the residue function (such as a decaying exponential, which corresponds physiologically to a well-mixed single compartment). This assumption works well if the true residue function corresponds to that selected, but errors occur when this is not the case.[17] Nondeconvolution methods base hemodynamic estimates on parameters derived exclusively from the tissue concentration curves, such as the maximal slope or the peak enhancement of the contrast enhancement curve. Some of these methods are easy to apply and are repeatable but usually entail very high rates of contrast agent injection (>5 mL/s), yield relative rather than absolute measurements, and depend strongly on the precise imaging parameters used. As such, these results are difficult to compare between institutions and will not be discussed further.

Once CBF and CBV are known, mean transit time (MTT) can be calculated, being the ratio of CBV and CBF, a property

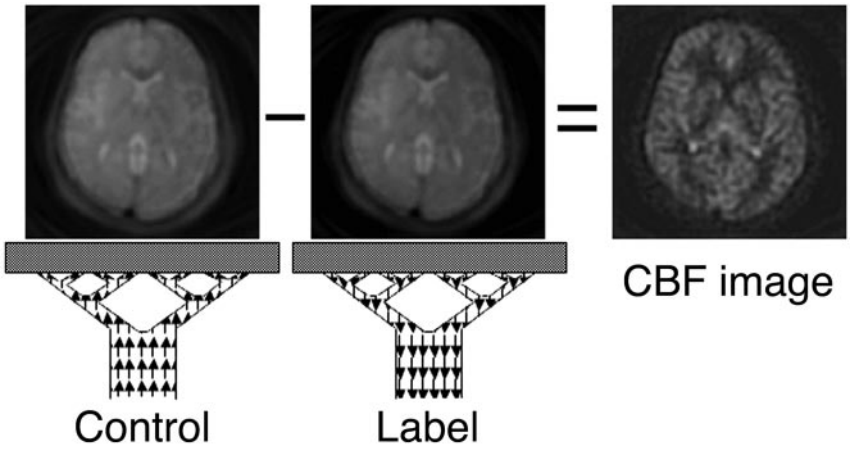

Fig 3. In ASL, upstream blood protons are either unperturbed (control) or inverted (label) on alternate applications of the pulse sequence, here demonstrated by the up arrows and down arrows, respectively. The signal intensity of the labeled images is approximately 1–2% lower than that of the control images due to the extraction of the negatively magnetized inverted spins into the tissue when they reach the capillary bed. Subtracting label images from control images creates a difference image proportional to CBF. Typically many such image pairs must be subtracted to achieve adequate SNR; the image of CBF in a healthy volunteer shown above was acquired in 5 minutes at 3T.

of tracers known as the central volume principle.[23] The MTT is the average time it takes for a contrast molecule to traverse the imaging voxel. In theory, MTT can be directly measured as the first moment of the residue function, though in practice this is challenging in the presence of noise and bolus delay. MTT is a very desirable measurement because gray matter and white matter have approximately equal MTT, leading to "flat contrast" for normal tissue. Abnormal tissue is much more apparent against such a background, and for this reason, MTT is the most sensitive marker of hemodynamic abnormality. In fact, it can sometimes be "too sensitive," in that not all regions of MTT abnormality appear to be at risk of infarction in acute stroke, and 150% of contralateral (presumed normal) brain tissue has been proposed as a threshold for "at risk" tissue.[24] Another hemodynamic parameter that has shown promise in acute stroke studies is the time at which the calculated residue function reaches its maximum (T_{max}), which exaggerates the effects of widening ("dispersion") and delay of the bolus between the AIF and the voxel.[25,26] However, T_{max} is really just an improved estimate of the delay in bolus arrival time between the AIF and the voxel and does not describe the hemodynamic status of the tissue itself.

Dispersion and delay between the measured AIF and the true inflow to the voxel can cause errors in PWI estimates of hemodynamic parameters. These errors are complex and can cause either over- or underestimation of CBF, depending on the delay between the AIF and the tissue.[27] A more recent formulation known as block circulant SVD[28] is theoretically immune to differences in bolus arrival time but still cannot account for dispersion. It has been shown to be theoretically equivalent to the previously mentioned Fourier method while preserving the desirable noise properties of SVD deconvolution.

Arterial Spin-Labeling

In contrast to bolus PWI, arterial spin-labeling (ASL) methods do not use contrast and measure CBF only.[29,30] Water is a diffusible tracer and shares many advantages with classic tracer methods such as positron-emission tomography (PET) or xenon CT (Xe-CT) measurements. Radio-frequency pulses are used to invert (or "label") water protons in the blood proximal to the imaged sections. This labeled water then flows distally, where it is extracted into the brain parenchyma at the capillary level. Imaging is then performed, typically by using rapid proton density–weighted images. The inflow of the label brings negative magnetization, which mixes with the static tissue positive magnetization and results in a small decrease in signal intensity of approximately 1–2%. A control acquisition identical to the labeled acquisition is obtained without water labeling. Flow-weighted images are created by subtracting the labeled images from the control images, thus in theory, removing the static tissue signal intensity (Fig 3). The advantages of ASL are the lack of ionizing radiation or contrast material injection, its flexibility and repeatability, and the relative availability of MR imaging compared with PET or Xe-CT. Also, the ability to image quantitative CBF from individual arteries has been demonstrated with this technique and could have applications to bypass surgery or to assess the functional significance of arterial stenoses.[31,32] The major disadvantage of ASL is the low SNR, which requires 5–10 minutes of MR imaging time at clinical field strengths of 1.5T and erroneous low CBF measurements and artifacts in regions with delayed blood arrival.

ASL sequences can be broken down into 2 sections: the labeling period and the imaging period. Initially, 2D EPI was used for image acquisition, given its efficient coverage of *k*-space and high SNR; more recently, approaches by using fast spin-echo and/or background suppression have shown promise to reduce susceptibility artifacts and noise from the static tissue.[33,34] Also, because spin-echo pulse sequences may be used, visualization of high-susceptibility areas, such as the inferior frontal and temporal lobes, is improved compared with that of gradient-echo PWI.

Two basic strategies are used to label the blood, known as pulsed and continuous. For maximal SNR, the inflowing blood protons are inverted. This can be accomplished by using a short radio-frequency pulse, an approach known as "pulsed ASL," (PASL).[35,36] An alternative, "continuous ASL" (CASL) creates a proximal plane by using off-resonance radio-frequency power and gradients to adiabatically invert flowing water.[29,37] In general, CASL has higher SNR than PASL but is more hardware and specific absorption rate (SAR) intensive. More recently, so-called pseudocontinuous ASL has been demonstrated, in which the continuous radio-frequency and gradient pulses are chopped into shorter lengths. This has been shown to maintain high labeling efficiency with significant decreases in SAR and hardware requirements and probably represents the wave of the future for high-field clinical ASL.[38] A final method, velocity-selective ASL, labels spins on

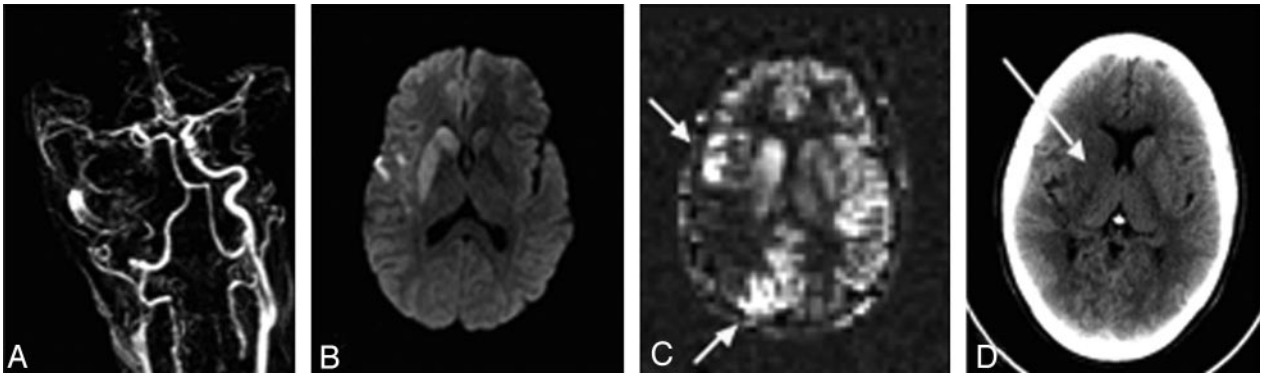

Fig 4. CBF errors due to prolonged arrival time in ischemic stroke with ASL. *A,* A contrast-enhanced MR angiogram shows right internal carotid artery occlusion. *B,* Diffusion-weighted image demonstrates abnormality of the right putamen, caudate, and a small area in the right frontal operculum. *C,* A PASL image of CBF demonstrates punctate high signal intensity (*arrows*) surrounding an area of apparent low flow in the right parietal lobe. The high signal intensity is probably due to delayed arrival of the label via collateral flow which is still within large vessels rather than in the parenchyma. The low measured CBF centrally is due to decay of the label before it enters the tissue. Normal flow was seen in this region on Xe-CT (images not shown). *D,* Follow-up CT 2 days later demonstrates infarction of the right caudate and putamen (*arrow*) but preserved gray-white contrast in the right parietal region that demonstrates low signal intensity on the ASL CBF map. CBF underestimation in the setting of collateral flow is a fundamental difficulty with the use of standard ASL in this patient population.

the basis of velocity rather than location and, as such, is theoretically insensitive to differences in arterial arrival times[39]; it is currently a research technique and beyond the scope of this article but has great promise as a truly quantitative CBF method, particularly in patients with cerebrovascular disease and extensive collateralization.

Quantifying CBF with ASL

The following discussion of the ASL signal intensity assumes that the labeled protons remain in small blood vessels at the time of imaging, the so-called microsphere model.[40] This model is emphasized here due to its simplicity, but more complex models that include the effects of exchange between the blood and tissue water have also been developed.[41]

The Bloch equation for longitudinal magnetization, with additional terms for the inflow and outflow of magnetization, is as follows:

$$6) \qquad \frac{dM_z(t)}{dt} = \frac{M_0 - M_z(t)}{T_1} + fM_{art}(t) - fM_{ven}(t),$$

where $M_z(t)$ is the longitudinal magnetization at time t, M_0 is the equilibrium magnetization in the absence of radio-frequency pulses, f is CBF, M_{art} is the inflowing arterial longitudinal magnetization at time t, and M_{ven} is the outflowing venous magnetization. T_1 may be considered the blood T_1, because the label spends most of its time there. M_{art} is the following:

$$7) \qquad M_{art}(t) = M_{0,blood}(1 - 2\alpha),$$

where α is the spin-labeling efficiency, which ranges from 0 to 1, with 0 signifying no labeling and 1 signifying perfect inversion, and $M_{0,blood}$ is the equilibrium magnetization of the blood. The mean residence time of a water proton is about 1 minute (which is much longer than the blood or tissue T_1), so the assumption is often made that M_{ven} is equal to the average tissue magnetization. This is a good assumption usually, though it fails in the setting of high CBF (>100 mL/100 g per minute), where the outflowing magnetization would include nonextracted but labeled spins. With the additional simplification that the equilibrium tissue and blood magnetization are approximately equal, Eq 6 becomes the following:

$$8) \qquad \frac{dM_z(t)}{dt} = \frac{M_0 - M_z(t)}{T_1} + f\left[(1 - 2\alpha)M_0 - M_z(t)\right].$$

To better understand the magnitude of the ASL signal intensity, we can solve this equation for the steady-state condition, when $dM_z(t)/dt$ is 0. This corresponds to the expected magnetization following infinite time duration either without or with labeling:

9) for $\alpha = 0$ (no labeling, control),

$$M_z^{control}(t \rightarrow \infty) = M_0,$$

10) for non-zero α (labeling):

$$M_z^{label}(t \rightarrow \infty) = \left(\frac{1 - (\alpha f T_1)}{1 + (\alpha f T_1)}\right) M_0.$$

This shows that the magnetization following the labeling experiment is smaller than that of the control acquisition, as expected, because the labeling is injecting inverted (negative) magnetization into the voxel. The difference between the label and control acquisitions (ΔM) is just

$$11) \qquad \Delta M(t \rightarrow \infty) = \frac{2\alpha f T_1}{1 + \alpha f T_1} M_0 \approx 2\alpha f T_1 M_0.$$

The last partial equality takes into account that the dimensionless term (fT_1), for a typical flow rate of 50 mL/100 g per minute is quite small (0.011). This explains why ASL difference signals are on the order of 1% of the equilibrium magnetization under the best conditions (ie, perfect labeling, no delays) and why ASL requires extensive signal averaging to achieve adequate SNR. Additionally, it shows why ASL is especially improved at 3T compared with 1.5T: The equilibrium blood magnetization doubles and the label persists longer due to the 30% increased blood T_1. Eq 11 gives the maximal-difference signal intensity for a CASL experiment; it can be shown that the maximal-difference signal intensity for a PASL experiment is

$$12) \qquad \Delta M_{PASL}(t \rightarrow \infty) \approx 2\alpha f T_1 M_0 e^{-1}.$$

Comparing Eqs 11 and 12 explains why CASL experiments are generally considered to have higher SNR than PASL experi-

ments, though in reality, this is more complicated, and theoretic and experimental results suggest that the SNR/unit time improvement between CASL and PASL is on the order of 20%–40% rather than this larger factor of e.[42,43]

CBF quantification errors can occur due to delays in arterial arrival time (Δt), which is defined as the time between proximal labeling and subsequent extraction into the tissue at the capillary level. If arrival times were uniform and known, they could be easily corrected by including the effects of T_1 relaxation within the blood upon M_{art}:

$$M_{art} = M_{0,blood}(1 - 2\alpha\exp(-\Delta t/T1_{blood})). \quad 13)$$

Although longer arterial arrival times would mean lower SNR images, quantification would not be affected. However, in reality, arterial arrival times are regionally dependent and difficult to measure accurately, but are typically on the order of 300–2000 ms, with the longer times seen in the white matter and vascular border zones.[44] Because this is on the order of the label T_1, large CBF underestimations can occur. Some investigators propose acquiring ASL difference images at different inflow times to directly estimate both Δt and CBF; however, this is usually time-consuming and the results can be confusing due to label remaining in feeding arteries during early inflow times (Fig 4) and in general leads to noisy images that are challenging to fit in a robust fashion.[45] Alternatively, one can design the pulse sequence such that the labeled blood has a well-defined temporal width, which is entirely delivered to the tissue before imaging. With PASL, this is typically performed by using a variant of the Quantitative Imaging of Perfusion Using a Single Subtraction Method 2 (QUIPSS 2), in which saturation pulses applied to the labeled region permit quantitative CBF measurements during a range of expected arrival times.[46]

With CASL, the same function is accomplished by inserting a delay time between the end of the labeling period and the start of imaging.[47] Conceptually, this allows late-arriving labeled spins to "catch up" with their earlier arriving counterparts. Both approaches incur decreased SNR in the hopes of improved quantification. High-field ASL will benefit from the ability to visualize later arriving spins due to higher SNR and longer blood T1. Arrival times on the order of 2 seconds in the watershed white matter and as long as 6–10 seconds in the setting of collateral flow, ischemic stroke, or extracranial-to-intracranial bypass are a significant challenge to standard quantitative ASL imaging in these patient populations. Because prolonged arrival times lead to decreased ASL signal intensity, in theory, this causes greater contrast between normal and abnormal regions in ischemic stroke, which may itself be a useful, albeit qualitative, measure that could be exploited for clinical imaging.

Permeability Imaging

Permeability describes how easy it is for a molecule to move between 2 separate environments separated by a well-defined barrier. For clinical MR imaging, the molecule of interest is the gadolinium-based contrast agent. The 2 separate environments are the intravascular and extracellular extravascular space (EES), and the barrier is the cerebrovascular endothelium (BBB) (Fig 5). This measurement is of interest because this permeability is essentially zero for regions with an intact BBB and nonzero in many pathologic situations, such as neoplasm, inflammatory/infectious disease, and ischemia. Postcontrast T1 enhancement can be seen, therefore, as a "snapshot" in the dynamic process in which contrast agents enter and exit the EES (they are thought to be excluded from cells). As long as there is a higher concentration of contrast in the blood than in the EES, contrast flows into the EES. With time, the concentration in the blood decreases, due to clearance by the kidneys and removal into the EES throughout the body. Once the EES and blood concentrations are equal, there will be no net flux; from this point onward, contrast will flow down the concentration gradient from the EES back into the blood and then finally will be excreted via the kidneys or sequestered in the reticular endothelial system.

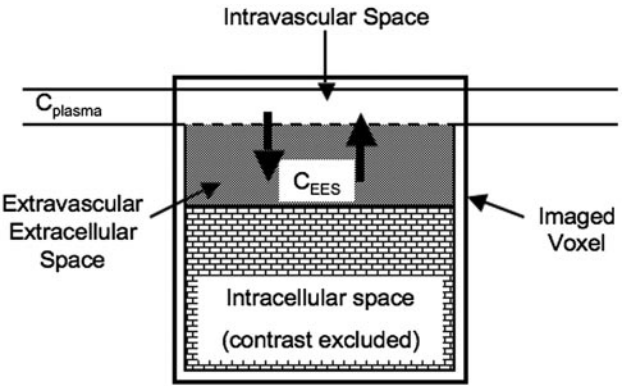

Fig 5. A basic model of the imaging voxel for permeability studies. The plasma volume, v_p, is small compared with the EES (shown in gray) and the intracellular space, from which contrast is excluded. Observed relaxivity changes are a weighted average of the plasma and EES contrast concentration. The large black arrows signify isodirectional flux of contrast between these 2 spaces, with a rate constant equal to K_{trans}. This flux is essentially zero in the presence of an intact BBB but is nonzero in many pathophysiologic conditions.

Specifically, permeability is defined as the bulk flow of a tracer normalized for surface area, concentration gradient, and time:

$$\frac{dC_{tissue}}{dt} = P \cdot S \cdot M \cdot (C_{plasma} - C_{EES}), \quad 14)$$

where P is the permeability (centimeters per second); S, the surface area per unit mass (square centimeters per gram); M, the tissue mass (gram); and $C_{plasma} - C_{EES}$, the concentration difference between the 2 compartments (millimoles per cubic centimeter). Because there is no direct way to separate the effects of changes in surface area from permeability, usually they are lumped together as the "PS product," which may then be compared among different parts of the brain. PS has the units of a rate constant, like flow. Eq 14 can be written as

$$\frac{dC_{tissue}}{dt} = PS\rho(C_{plasma} - (C_{tissue}/v_e)), \quad 15)$$

where ρ is the brain density. Note that the ratio of C_{tissue} and the EES volume fraction v_e is just the "true" EES concentration.

At this point, it is important to point out an important simplification of the model: to fit the previous equation, we need to know the plasma tracer concentration at the site of exchange (capillaries), which we will estimate from the arterial

concentration. However, it is possible that the PS product is large enough such that the concentration might change between the arterial and venous sides of the capillary. This occurs when the PS product (which describes the leakage of tracer during the passage) is of the same magnitude as the CBF. Because it is difficult to know the exact relationship between these parameters, a new quantity, the "transport constant" (K_{trans}), is used in place of the PS term in Eq 15 when fitting plasma and tissue concentration curves:

$$16) \qquad \frac{dC_{tissue}}{dt} = K_{trans}(C_{plasma} - (C_{tissue}/\nu_e)),$$

where in the extreme cases

$$17) \quad K_{trans} = CBF \cdot (1 - Hct) \qquad \text{if} \qquad f << PS,$$

$$18) \qquad K_{trans} = PS\rho \qquad \text{if} \qquad f >> PS.$$

Eq 17 more accurately represents the situation for most neoplasms, where leakage concentrations are limited by the contrast delivery rate (ie, CBF limited). Eq 18 is more accurate in the setting of lower permeability seen in ischemia and inflammatory diseases such as chronic multiple sclerosis plaques, where the contrast leakage is not limited by delivery (permeability limited).

Given this basic model, how does one determine the plasma and tissue concentrations, which are needed to calculate K_{trans} and v_e? Plasma concentration can be either directly measured (in which case it is similar to the AIF described in the bolus section) or assumed as a biexponential decay curve.[48] The first of these methods may require additional imaging and is prone to errors from inflow and partial volume. The latter method is unlikely to account for differences in patient size and renal clearance. To convert between tissue concentration and relaxation changes, one assumes a model of fast exchange throughout. Two basic methodologies for extracting K_{trans} and other hemodynamic variables are described below.

Steady-State T1 Method

Tofts and Kermode[49] have studied a steady-state T1-based model (ssT1, sometimes termed the "pharmacokinetic model"), in which repeated short TE, T1-weighted images are acquired before and after contrast injection. Comparison with baseline precontrast images and knowledge of the initial R_1 (inverse of $T1$) and TR of the measurement allows an iterative solution of the R_1 change (ΔR_1):

$$19) \qquad \frac{S(t)}{S_0} = \frac{1 - \exp([R_1 + \Delta R_1]TR)}{1 - \exp(R_1 TR)}.$$

As for dynamic susceptibility contrast bolus measurements, ΔR_1 is assumed to be linearly proportional to contrast concentration. Figure 6 describes how plasma and tissue signal intensities change with time for a range of K_{trans}.

Relaxivity change occurs in 2 compartments, the plasma and the EES, because the contrast agent is excluded from the intracellular space. Thus, the tissue concentration is a weighted average of these 2:

$$20) \qquad C_{tissue}(t) = \nu_p C_{plasma}(t) + \nu_e C_{EES}(t),$$

where ν_p again represents the plasma volume (CBV · [1 − Hct]). Because both plasma volume and concentration (at least several minutes following the bolus first pass) are low, the plasma term is ignored. Then Eq 16 is rewritten in terms of C_{EES}:

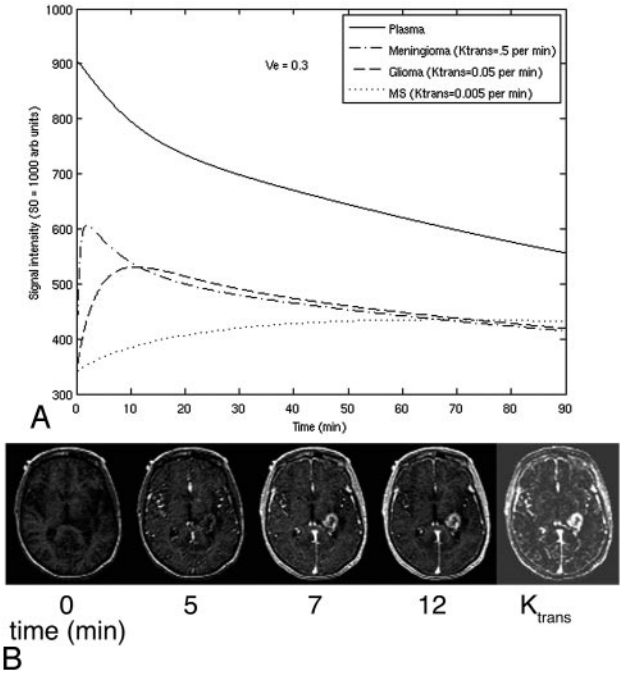

Fig 6. *A*, Simulated signal-intensity enhancement curve versus time by using the steady-state T1 method for tissue with different permeability, corresponding to a meningioma (K_{trans} = 0.5/min), a glioma (K_{trans} = 0.05/min), and a chronic multiple sclerosis (MS) lesion (K_{trans} = 0.005/min). v_e of 0.3 is assumed. Proton density is assumed to be 1,000 arbitrary units (au) for all tissue, T1 before contrast is 1.2 seconds, and a typical spin-echo T1-weighted sequence with a TR of 500 ms is assumed. Note the rapid rise and subsequent fall of signal intensity in the highly leaky meningioma compared with the more gradual onset of contrast enhancement in the MS lesion. As is typical for the ssT1 method, contribution from the intravascular space is neglected. *B*, An example of gradual enhancement on T1-weighted imaging in a high-grade glioma at several time points following contrast administration by using the ssT1 method. The fitted K_{trans} permeability map is shown at the right. Image courtesy of Dr. Soonmee Cha, University of California, San Francisco.

$$21) \qquad \nu_e \frac{dC_{EES}}{dt} = K_{trans}(C_{plasma} - C_{EES}),$$

which can be solved as an integral and inserted into Eq 20, ignoring plasma contributions:

$$22) \qquad C_{tissue}(t) = K_{trans} \int_0^t C_{plasma}(\tau) e^{-K_{trans}(t-\tau)/\nu_e} d\tau.$$

This equation is then fitted in each voxel by using nonlinear least squares methods to determine K_{trans} and ν_e.

First-Pass Methods

Because the ssT1 method requires sequential imaging for many minutes (sometimes hours), which can be difficult in the clinical setting, several groups have tried to fit the signal intensity during the first pass of a contrast bolus and the early recirculation period to account for permeability. This has the advantage that the data acquisition is faster and, in fact, is a standard part of the clinical work-up to measure plasma volume, as described previously. Two models will briefly be discussed here. Both attempt to determine the signal intensity

that would be measured in the absence of permeability, by examining the concentration time curves of brain tissue thought to be free of disease, such as normal-appearing white matter contralateral to the lesion being evaluated. Then, the difference between the observed and expected concentration curve is attributed to the effects of changes in plasma volume, EES volume fraction, and permeability.

Both models assume that the relationship between concentration and $\Delta R2^*$ is the same whether the contrast remains in the vasculature or has leaked out into the EES. This is problematic because the fundamental idea behind dynamic susceptibility contrast rests on the idea that high $\Delta R2^*$ changes are due to sequestration of contrast within vessels,[1] thus creating local magnetic field gradients (in addition to bulk susceptibility changes). Contrast in the EES could serve to decrease these magnetic field gradients, causing paradoxically, lower relaxivity, or at minimum, a change in the relationship between $\Delta R2^*$ and tissue concentration.[50] It has been suggested that the agent is still somewhat sequestered, being excluded from the intracellular space,[51] though this remains a difficult assumption to test.

The first model was described by Weisskoff et al[52] and was subsequently elaborated by Donahue et al.[3] It focuses on the effects of the T1 changes that occur when contrast leaks. Because rapid EPI images are T1- as well as T2*-weighted, reductions in T1 will tend to increase signal intensity. The relationship between the "apparent" and true transverse relaxivity changes can be shown to be related to the baseline $R_1 (= 1 / T_1)$ and the *TR* and *TE* of the sequence:

$$23) \quad \Delta R^*_{2,measured}(t) = \Delta R^*_2(t) - \frac{TR\exp(-TR/T_1)}{TE(1-\exp(-TR/T_1)}R_1 C_{tissue}(t).$$

They ignored possible flow of contrast from the tissue back into the plasma, so the contribution of this latter term only increases with time on the basis of the average amount of exposure it has had to the contrast in the plasma:

$$24) \quad C_{tissue}(t) = kK_{trans}\int_0^t \overline{\Delta R^*_2(\tau)}d\tau,$$

where the overbar signifies a spatial average over all voxels that do not show postcontrast enhancement (presumably those with zero permeability), and *k* is a constant that converts from units of relaxivity to concentration. Then, nonlinear least squares fitting is applied to calculate the coefficients corresponding to a term proportional to plasma concentration (related to plasma volume) and a term linear with this integral (which incorporates the effects of permeability).

Another approach was suggested by Johnson et al,[51] known as the first-pass T2* method or first-pass parametric model, and theoretically yields estimates of v_p, v_e, and K_{trans}. It assumes that T1 effects are small during bolus passage and in the immediate recirculation period and may be neglected. For the T1 criteria to be satisfied, they suggested that the sequences should be made less T1-sensitive by lowering the flip angles (to 30° rather than 90°), though this results in decreased SNR; another approach would be to directly measure and correct by using multiple echoes.[4] Recalling Eq 20 and explicitly including plasma contributions to tissue concentration yields the following equation:

$$25) \quad C_{tissue}(t) = v_p C_{plasma} + K_{trans}\int_0^t C_{plasma}(\tau)e^{-K_{trans}(t-\tau)/v_e}d\tau.$$

While recast in terms of concentration, this equation is quite similar to that of Donahue et al,[3] with the exception that back flow of contrast from the EES into the tissue is permitted. This allows estimation of the EES volume fraction v_e at the expense of adding an additional free parameter to an already ill-posed nonlinear least squares fitting algorithm. Again, as in the previous approach, the plasma concentration is estimated from presumed normal tissue with zero permeability, in this case, normal-appearing contralateral white matter and a literature-derived plasma volume of 1 mL/100 g. This method was shown to yield good correlation with the ssT1 method in gliomas, but with no correlation in more leaky meningiomas.[50] Simulations of these models suggest that K_{trans} may be somewhat overestimated and plasma volume somewhat underestimated.[53]

Studies of permeability by using first-pass kinetics are likely in their infancy. However, given the ubiquity of the bolus method, derivation of these additional hemodynamic parameters may have significant clinical impact. In the end, it is likely that the "best" model to fit the data depends on the precise T1 and T2* weighting of the pulse sequence. Direct comparison of these methods to gold standard methods of permeability should be a priority to establish these methods as reliable and reproducible.

Conclusions

Dynamic susceptibility contrast, ASL, and methods to measure permeability represent the effort of many research and clinical MR imaging scientists, who believe that quantitative physiologic imaging of the brain can help in the identification and treatment of disease. A basic theoretic understanding of these techniques may help speed their acceptance into routine clinical practice.

Acknowledgments

I thank Drs. Roland Bammer and Michael E. Moseley for valuable discussions and critiques of initial drafts of this manuscript.

References

1. Fisel CR, Ackerman JL, Buxton RB, et al. **MR contrast due to microscopically heterogeneous magnetic susceptibility: numerical simulations and applications to cerebral physiology.** *Magn Reson Med* 1991;17:336–47
2. Kiselev VG. **On the theoretical basis of perfusion measurements by dynamic susceptibility contrast MRI.** *Magn Reson Med* 2001;46:1113–22
3. Donahue KM, Krouwer HG, Rand SD, et al. **Utility of simultaneously acquired gradient-echo and spin-echo cerebral blood volume and morphology maps in brain tumor patients.** *Magn Reson Med* 2000;43:845–53
4. Miyati T, Banno T, Mase M, et al. **Dual dynamic contrast-enhanced MR imaging.** *J Magn Reson Imaging* 1997;7:230–35
5. Barbier EL, den Boer JA, Peters AR, et al. **A model of the dual effect of gadopentetate dimeglumine on dynamic brain MR images.** *J Magn Reson Imaging* 1999;10:242–53
6. Weisskoff R, Zuo C, Boxerman J, et al. **Microscopic susceptibility variation and transverse relaxation: theory and experiment.** *Magn Reson Med* 1994;31:601–10
7. Zaharchuk G, Mandeville JB, Bogdanov AA Jr, et al. **Cerebrovascular dynamics of autoregulation and hypoperfusion: an MRI study of CBF and changes in**

total and microvascular cerebral blood volume during hemorrhagic hypotension. *Stroke* 1999;30:2197–205
8. Zaharchuk G, Yamada M, Shimizu-Sasamata M, et al. **Is all perfusion-weighted magnetic resonance imaging for stroke equal? The temporal evolution of multiple hemodynamic parameters after focal ischemia in rats correlated with evidence of infarction.** *J Cereb Blood Flow Metab* 2000;20:1341–51
9. Dennie J, Mandeville JB, Boxerman JL, et al. **NMR imaging of changes in vascular morphology due to tumor angiogenesis.** *Magn Reson Med* 1998;40:793–99
10. Lassen NA, Perl W. *Tracer Kinetic Methods in Medical Physiology*. New York: Raven Press; 1979
11. Kety SS, Schmidt CF. **The determination of cerebral blood flow in man by the use of nitrous oxide in low concentrations.** *Am J Physiol* 1945;143:53–66
12. Yen RT, Fung YC. **Inversion of Fahraeus effect and effect of mainstream flow on capillary hematocrit.** *J Appl Physiol* 1977;42:578–86
13. Hunter GJ, Hamberg LM, Ponzo JA, et al. **Assessment of cerebral perfusion and arterial anatomy in hyperacute stroke with three-dimensional functional CT: early clinical results.** *AJNR Am J Neuroradiol* 1997;19:29–37
14. Powers WJ. **Cerebral hemodynamics in ischemic cerebrovascular disease.** *Ann Neurol* 1991;29:231–40
15. de Crespigny A, Rother J, van Bruggen N, et al. **Magnetic resonance imaging assessment of cerebral hemodynamics during spreading depression in rats.** *J Cereb Blood Flow Metab* 1998;18:1008–17
16. Zierler K. **Theoretical basis of indicator-dilution methods for measuring flow and volume.** *Circ Research* 1962;10:393–407
17. Ostergaard L, Weisskoff RM, Chesler DA, et al. **High resolution measurement of cerebral blood flow using intravascular tracer bolus passages. Part I. Mathematical approach and statistical analysis.** *Magn Reson Med* 1996;36:715–25
18. Alsop DC, Wedmid A, Schlaug G. **Defining a local arterial input function for perfusion quantification with bolus contrast MRI.** *Proceedings of Tenth Scientific Meeting and Exhibition of the International Society for Magnetic Resonance in Medicine, May 18–24, 2002.* Honolulu, Hawaii: ISMRM; 2002:659
19. Lorenz C, Benner T, Lopez CJ, et al. **Effect of using local arterial input functions on cerebral blood flow estimation.** *J Magn Reson Imaging* 2006;24:57–65
20. Jochimsen TH, Newbould RD, Skare ST, et al. **Identifying systematic errors in quantitative dynamic-susceptibility contrast perfusion imaging by high-resolution multi-echo parallel EPI.** *NMR Biomed* 2007;20:429–38
21. Rempp KA, Brix G, Wenz F, et al. **Quantitation of cerebral blood flow and volume with dynamic susceptibility contrast-enhanced MR imaging.** *Radiology* 1994;193:637–41
22. Bretscher O. *Linear Algebra with Application.* 3rd ed. Upper Saddle River, NJ: Pearson Prentice Hall; 2005
23. Stewart GN. **Researches on the circulation time in organs and on the influences which affect it. Parts I-III.** *J Physiol (London)* 1894;15:1
24. Wintermark M, Flanders AE, Velthuis B, et al. **Perfusion-CT assessment of infarct core and penumbra: receiver operating characteristic curve analysis in 130 patients suspected of acute hemispheric stroke.** *Stroke* 2006;37:979–85
25. Shih LC, Saver JL, Alger JR, et al. **Perfusion-weighted magnetic resonance imaging thresholds identifying core, irreversibly infarcted tissue.** *Stroke* 2003;34:1425–30
26. Albers GW, Thijs VN, Wechsler L, et al. **Magnetic resonance imaging profiles predict clinical response to early reperfusion: the diffusion and perfusion imaging evaluation for understanding stroke evolution (DEFUSE) study.** *Ann Neurol* 2006;60:508–17
27. Calamante F, Gadian DG, Connelly A. **Delay and dispersion effects in dynamic susceptibility contrast MRI: simulations using singular value decomposition.** *Magn Reson Med* 2000;44:466–73
28. Wu O, Ostergaard L, Weisskoff RM, et al. **Tracer arrival timing-insensitive technique for estimating flow in MR perfusion-weighted imaging using singular value decomposition with a block-circulant deconvolution matrix.** *Magn Reson Med* 2003;50:164–74
29. Dixon WT, Du LN, Faul DD, et al. **Projection angiograms of blood labelled by adiabatic fast passage.** *Magn Reson Med* 1986;3:454–62
30. Detre JA, Leigh JS, Williams DS, et al. **Perfusion imaging.** *Magn Reson Med* 1992;23:37–45
31. Zaharchuk G, Ledden P, Kwong K, et al. **Multislice perfusion and perfusion territory imaging in humans with separate label and image coils.** *Magn Reson Med* 1999;41:1093–98
32. Hendrikse J, van der Grond J, Lu H, et al. **Flow territory mapping of the cerebral arteries with regional perfusion MRI.** *Stroke* 2004;35:882–87
33. Guenther M, Oshio K, Feinberg DA. **Single-shot 3D imaging techniques improve arterial spin labeling perfusion measurements.** *Magn Reson Med* 2005;54:491–98
34. Garcia DM, Duhamel G, Alsop DC. **Efficiency of inversion pulses for background suppressed arterial spin labeling.** *Magn Reson Med* 2005;54:366–72
35. Edelman R, Siewert B, Darby D, et al. **Qualitative mapping of cerebral blood flow and functional localization with echo-planar MR imaging and signal targeting with alternating radio frequency.** *Radiology* 1994;192:513–20
36. Kwong KK, Chesler DA, Weisskoff RM, et al. **MR perfusion studies with T1-weighted echo planar imaging.** *Magn Reson Med* 1995;34:878–87
37. Roberts DA, Detre JA, Bolinger L, et al. **Quantitative magnetic resonance imaging of human brain perfusion at 1.5 T using steady-state inversion of arterial water.** *Proc Natl Acad Sci U S A* 1994;91:33–37
38. Garcia DM, de Bazelaire C, Alsop DC. **Pseudo-continuous flow-driven adiabatic inversion for arterial spin labeling.** *Proceedings of Thirteenth Scientific Meeting and Exhibition of the International Society for Magnetic Resonance in Medicine, May 7–13, 2005.* Miami, Fla: ISMRM; 2005:37
39. Wong EC, Cronin M, Wu W-C, et al. **Velocity-selective arterial spin labeling.** *Magn Reson Med* 2006;55:1334–41
40. Buxton RB, Frank LR, Wong EC, et al. **A general kinetic model for quantitative perfusion imaging with arterial spin labeling.** *Magn Reson Med* 1998;40:383–96
41. Parkes LM, Tofts PS. **Improved accuracy of human cerebral blood perfusion measurements using arterial spin labeling: accounting for capillary water permeability.** *Magn Reson Med* 2002;48:27–41
42. Wong EC, Buxton RB, Frank LR. **A theoretical and experimental comparison of continuous and pulsed arterial spin labeling techniques for quantitative perfusion imaging.** *Magn Reson Med* 1998;40:348–55
43. Wang J, Alsop DC, Li L, et al. **Comparison of quantitative perfusion imaging using arterial spin labeling at 1.5 and 4.0 Tesla.** *Magn Reson Med* 2002;48:242–54
44. Wong EC, Buxton RB, Frank LR. **Implementation of quantitative perfusion imaging techniques for functional brain mapping using pulsed arterial spin labeling.** *NMR Biomed* 1997;10:237–49
45. Donahue MJ, Lu H, Jones CK, et al. **An account of the discrepancy between MRI and PET cerebral blood flow measure: a high-field MRI investigation.** *NMR Biomed* 2006;19:1043–54
46. Wong EC, Buxton RB, Frank LR. **Quantitative imaging of perfusion using a single subtraction (QUIPSS and QUIPSS II).** *Magn Reson Med* 1998;39:702–08
47. Alsop DC, Detre JA. **Reduced transit time sensitivity in noninvasive magnetic resonance imaging of human cerebral blood flow.** *J Cereb Blood Flow Metab* 1996;16:1236–49
48. Tofts PS. **Modeling tracer kinetics in dynamic Gd-DTPA MR imaging.** *J Magn Reson Imaging* 1997;7:91–101
49. Tofts PS, Kermode AG. **Measurement of the blood-brain barrier permeability and leakage space using dynamic MR imaging. 1. Fundamental concepts.** *Magn Reson Med* 1991;17:357–67
50. Cha S, Yang L, Johnson G, et al. **Comparison of microvascular permeability measurements, K(trans), determined with conventional steady-state T1-weighted and first-pass T2*-weighted MR imaging methods in gliomas and meningiomas.** *AJNR Am J Neuroradiol* 2006;27:409–17
51. Johnson G, Wetzel SG, Cha S, et al. **Measuring blood volume and vascular transfer constant from dynamic, T(2)*-weighted contrast-enhanced MRI.** *Magn Reson Med* 2004;51:961–68
52. Weisskoff RM, Boxerman JL, Sorensen AG, et al. **Simultaneous blood volume and permeability mapping using a single Gd-based contrast injection.** *Proceedings of the Twelfth Annual Meeting of the Society for Magnetic Resonance Imaging,* San Francisco, Calif; 1994:279
53. Buckley DL. **Uncertainty in the analysis of tracer kinetics using dynamic contrast-enhanced T1-weighted MRI.** *Magn Reson Med* 2002;47:601–06